Photochemical & Photobiological Sciences

PAPER

Cite this: *Photochem. Photobiol. Sci.*, 2019, **18**, 2766

Theoretical insight into the photophysical properties of six heteroleptic Ir(III) phosphorescent complexes bearing ppy-type ligands†

Deming Han, [a,b] Lihui Zhao[a] and Xuerong Han*[a]

Received 11th May 2019,
Accepted 30th September 2019

DOI: 10.1039/c9pp00218a

rsc.li/pps

By using density functional theory and time-dependent density functional theory, the geometrical, electronic and photophysical properties of six complexes with two ppy-type ligands and one acetylacetone anion around the Ir center have been explored. The lowest energy absorption wavelengths are located at 414 nm for **1**, 434 nm for **2**, 434 nm for **3**, 421 nm for **4**, 436 nm for **5**, and 425 nm for **6**, respectively. The lowest energy emissions of these complexes are localized at 617, 492, 633, 634, 491 and 491 nm, respectively, for complexes **1–6**, simulated in CH_2Cl_2 medium at the M062X level. The calculated lowest lying absorption wavelength and the lowest energy emission wavelength for complex **3** are very close to the available experimental values. The position and number of the incorporated electron-withdrawing fluorine substituents have some effect on the electronic and photophysical properties of these studied complexes.

1. Introduction

In the last two decades, organic light-emitting diodes (OLEDs) have been a hot research topic due to the requirement for full-color flat-panel displays and low-cost lighting sources.[1–6] It is well-known that because phosphorescent transition metal complexes are capable of harvesting both singlet and triplet excitons, phosphorescent emitters offer the potential to reach 100% internal quantum efficiency in OLEDs, while fluorescent emitters are limited to singlet excitons.[7] Many phosphorescent transition metal complexes, such as Ru(II), Rh(III), Os(II), Ir(III) and Pt(II) complexes, have attracted significant academic and industrial research interest due to their potential application in the fabrication of OLEDs;[8–16] especially, cyclometalated iridium(III) complexes are regarded as the most fascinating phosphors because of their unique photophysical properties, such as tunable emission energy, high phosphorescence efficiencies and short lifetimes.[17–23]

In recent years, the elements in group VIA have been widely employed to construct phosphorescent Ir(III) and Pt(II) complexes with 2-phenylpyridine (ppy)-type ligands. The hole injection/hole transport ability and electroluminescence efficiencies of these ppy-type Ir(III) and Pt(II) phosphorescent complexes have been enhanced through the strategy of attaching both phenyl ether and phenyl sulfide groups to them. Recently, Feng *et al.* have investigated the photophysical properties of a series of asymmetric heteroleptic Ir(III) phosphorescent complexes (Ir-Se0F, Ir-Se1F, Ir-Se2F, and Ir-Se3F) synthesized by using 2-selenophenylpyridine and one ppy-type (ppy = 2-phenylpyridine) ligand with a fluorinated selenide group.[24] In this study, on the basis of complex Ir-Se3F,[24] five complexes have been designed. Furthermore, by using density functional theory (DFT) and time-dependent density functional theory (TDDFT), the electronic structures, charge injection and transport, and spectral properties of these complexes have been theoretically studied. It is anticipated that this research could provide good guidance for the design of high performance ppy-type Ir(III) phosphorescent emitters.

2. Computational method

The ground state geometry for each molecule was optimized by the density functional theory (DFT)[25] method with a hybrid Hartree–Fock/density functional model (PBE0) based on the Perdew–Burke–Ernzerhof (PBE).[26] On the basis of the ground- and excited-state equilibrium geometries, the time-dependent DFT (TDDFT) approach was applied to investigate the absorption and emission spectral properties. The "double-ξ" quality basis set LANL2DZ[27,28] associated with the pseudopotential was employed for Ir atoms. The 6-31G(d,p) basis set was used

[a]*School of Life Science and Technology, Changchun University of Science and Technology, Changchun 130022, P.R. China. E-mail: hanxuerongcust@163.com*
[b]*Jilin Provincial Science and Technology Innovation Center of Optical Materials and Chemistry, Changchun, 130022, P.R. China*

†Electronic supplementary information (ESI) available. See DOI: 10.1039/c9pp00218a

for nonmetal atoms in the gradient optimizations. Furthermore, the stable configurations of these complexes can be confirmed by frequency analysis, in which no imaginary frequency was found for all configurations at the energy minima. All calculations were performed with the polarized continuum model (PCM) in CH_2Cl_2 medium. The calculated electron density plots for frontier molecular orbitals were prepared by using GaussView 5.0.8 software. All calculations were performed with the Gaussian 09 software package.[29]

3. Results and discussion

3.1 Geometries in the ground state S_0 and triplet excited state T_1

The sketch map of iridium(III) complexes **1–6** is presented in Fig. 1(a), and the partial atomic number of complex **1** as a representative is shown in Fig. 1(b). To gain a better understanding of the structural modification from the S_0 to T_1 state, the main optimized geometric parameters of S_0 and T_1 are presented in Table 1.

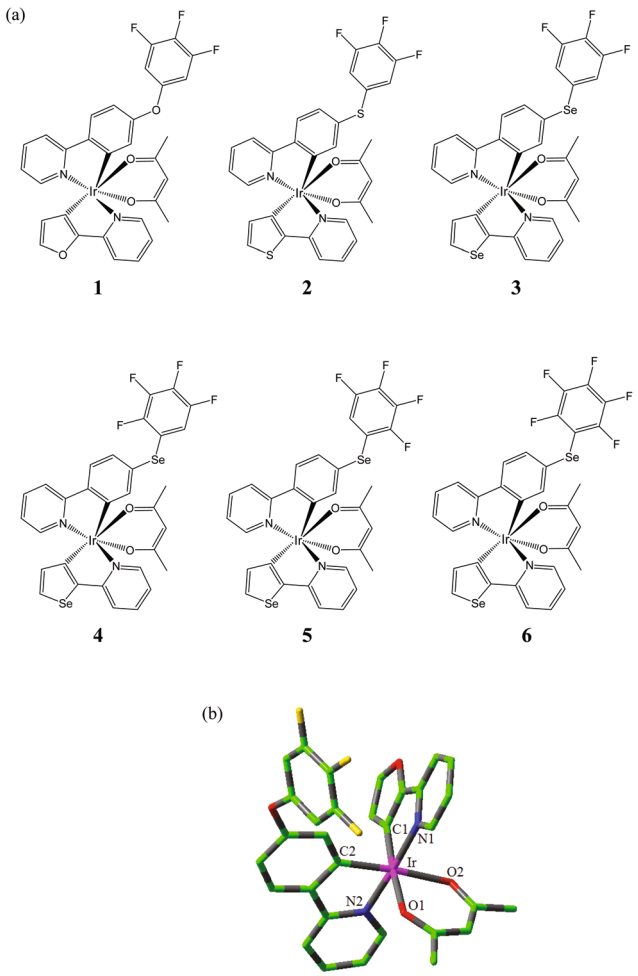

Fig. 1 (a) Sketch map of the structures of iridium(III) complexes **1–6**. (b) Representative optimized structure of complex **1** (H atoms omitted).

As depicted in Fig. 1(a), for complexes **1–6**, two ppy-type ligands and one acetylacetone anion around the Ir center furnish the chelating skeleton with *cis*-C,C, *cis*-O,O, and *trans*-N,N chelating disposition. For all these complexes, the bond lengths of Ir–C1 and Ir–C2 are between 1.90 and 1.99 Å, the bond lengths of Ir–N1 and Ir–N2 are between 2.00 and 2.09 Å, and the bond lengths of Ir–O1 and Ir–O2 are between 2.10 and 2.19 Å. The bond angles C1–Ir–O1, C2–Ir–O2 and N1–Ir–N2 for complexes **1–6** are more than 173°. The dihedral angles C1–C2–O1–O2, C1–N2–O1–N1 and C2–N2–O2–N1 for complexes **1–6** are less than 8°. This indicates that all these heteroleptic iridium complexes possess a distorted octahedral configuration. The position and number of the incorporated fluorine atoms are different from complex **3** to **6**, the geometrical structure parameters of which also show some slight changes.

In addition, to examine the changes of the geometrical structures upon excitation, the calculated geometrical parameters of the lowest lying triplet excited states (T_1) for all the studied complexes are also presented in Table 1. The bond lengths Ir–C1 for complexes **1–6** are slightly shorter, in contrast to those in the singlet state (S_0) when the other bond lengths show erratic changes. The bond angles C2–Ir–O2 and N1–Ir–N2 show a slight decrease and increase, respectively, compared with those of the S_0 state. The dihedral angles C1–C2–O1–O2 for complexes **1–6** are smaller than those of the S_0 state.

3.2 Molecular orbital properties

The detailed information of frontier molecular orbital (FMO) compositions for complexes **1–6** is presented in Tables S1–S6 (ESI†). The HOMO and LUMO distribution, energy levels, and energy gaps between of the LUMO and HOMO ($\Delta E_{L\rightarrow H}$) of **1–6** are also plotted in Fig. 2. In addition, Fig. S1† presents the names of different ligands in complexes **1–6** (taking complex **1** as an example).

From Fig. 2 and Tables S1–S6,† it can be seen that the HOMO of complexes **1–6** resides mainly on the Ir atom and L1 and L2 ligands. For example, the HOMO of **1** distributes over the d-orbital of Ir (33%) and the π-orbital of L1 (14%) and L2 ligands (50%). In addition, the HOMO energy levels for complexes **1–6** are not obviously different, that is, from −5.62 to −5.51 eV. The LUMO of complexes **1–6** resides mostly on the L1 ligand, for example, 94% antibonding π*-orbital of the L1 ligand for complex **1**. The LUMO energy levels for complexes **1–6** have some difference from −1.87 to −1.61 eV; especially, complex **1** has the largest HOMO, LUMO and $\Delta E_{L\rightarrow H}$ values (−5.51, −1.61 and 3.90 eV). In contrast, complex **5** has the smallest $\Delta E_{L\rightarrow H}$ value (3.73 eV). Comparing complex **4** with **5**, the HOMO, LUMO and $\Delta E_{L\rightarrow H}$ values of **4** are larger than those of **5**, which indicates that the different position of electron-withdrawing fluorine substituents has an obvious effect on the electronic structure properties.

3.3 Ionization potentials (IPs) and electronic affinities (EAs)

The good device performance of OLEDs is closely bound up with the excellent charge injection and transport abilities and

Table 1 Main optimized geometry parameters for complexes **1–6**

	1		**2**		**3**		**4**		**5**		**6**	
	S_0	T_1	S_0	T_1	S_0	T_1	S_0	T_1	S_0	T_1	S_0	T_1
Bond length (Å)												
Ir–C1	1.988	1.956	1.986	1.965	1.988	1.959	1.988	1.959	1.988	1.962	1.988	1.966
Ir–C2	1.986	1.990	1.987	1.963	1.986	1.989	1.989	1.992	1.987	1.967	1.989	1.964
Ir–N1	2.078	2.061	2.062	2.078	2.059	2.049	2.058	2.046	2.059	2.078	2.057	2.073
Ir–N2	2.038	2.047	2.041	2.030	2.041	2.046	2.042	2.048	2.041	2.028	2.042	2.032
Ir–O1	2.157	2.157	2.161	2.163	2.160	2.162	2.163	2.165	2.161	2.169	2.164	2.165
Ir–O2	2.171	2.183	2.168	2.167	2.168	2.181	2.169	2.181	2.168	2.163	2.168	2.167
Bond angle (°)												
C1–Ir–O1	173.79	174.76	174.71	174.11	174.66	175.74	174.65	175.62	174.85	175.21	174.42	173.81
C2–Ir–O2	175.17	175.10	175.05	174.01	174.28	173.87	175.12	175.10	174.28	171.23	174.81	173.13
N1–Ir–N2	176.11	176.61	176.14	177.14	176.09	176.69	176.49	177.06	176.29	176.84	176.48	177.15
Dihedral angle (°)												
C1–C2–O1–O2	7.21	6.03	6.59	4.78	6.74	5.53	6.67	5.39	6.68	5.54	7.03	5.39
C1–N2–O1–N1	2.39	2.60	2.37	3.12	2.23	2.40	2.26	2.60	1.85	1.69	2.42	3.31
C2–N2–O2–N1	3.58	3.85	3.68	5.61	4.63	5.01	3.22	3.44	4.64	7.97	3.17	6.06

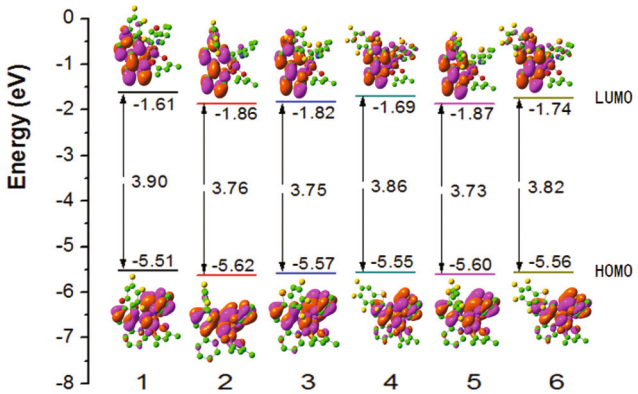

Fig. 2 Molecular orbital diagrams and HOMO and LUMO energies for complexes **1–6**.

the balance between the electron and hole transport. The ionization potential (IP) and electron affinity (EA) both in vertical (v, at the geometry of the neutral molecule) and adiabatic (a, optimized structures for both the neutral and charged molecules) processes have been investigated in order to quantitatively evaluate the charge injection abilities. The calculated vertical IP (IP_v), adiabatic IP (IP_a), vertical EA (EA_v), and adiabatic EA (EA_a) are also listed in Table 2.

As it is known that a smaller IP value facilitates hole injection, while a larger EA value will facilitate electron injection. The IP (both vertical and adiabatic) values for complexes **2** and **5** are larger than those of the other four complexes. In addition, the EA (both vertical and adiabatic) values of **5** are the largest among these complexes, which is beneficial to enhance the electron injection ability. According to the Marcus–Hush model,[30] the charge (hole or electron) transfer rate K_{et} can be expressed by the following formula:

$$K_{et} = A \exp(-\lambda/4k_B T) \quad (1)$$

where T is the temperature, k_B is the Boltzmann constant, and λ is the reorganization energy. Due to the limited intermolecular charge transfer range in the solid state, the mobility of charges has been demonstrated to be predominantly related to the internal reorganization energy λ for OLED materials.[31,32] Thus, at constant temperature, a low λ value is required for an efficient charge transport process. Herein, we focus on the inner reorganization energy λ_i, which is caused by the change of the internal nuclear coordinates from the reactant A to the product B and *vice versa* (Fig. 3). It can be expressed by the following formula:

$$\lambda_i = \lambda_0 + \lambda_1 = (E_B^A - E_A) + (E_A^B - E_B) \quad (2)$$

where E_A and E_A^B are the energies of A and B at the optimized geometry of A, respectively and E_B^A and E_B are the energies of A and B at the optimized geometry of B, respectively. The hole extraction potential (HEP) has been calculated, which is the

Table 2 The calculated vertical IP (IP_v), adiabatic IP (IP_a), hole extraction potential (HEP), vertical EA (EA_v), adiabatic EA (EA_a), electron extraction potential (EEP), and reorganization energies for electrons (λ_e) and holes (λ_h), unit: eV

	IP_v	IP_a	HEP	EA_v	EA_a	EEP	λ_e	λ_h
1	5.352	5.235	5.117	1.737	1.927	2.083	0.346	0.235
2	5.434	5.315	5.185	1.988	2.153	2.318	0.330	0.249
3	5.386	5.240	5.161	1.958	2.139	2.310	0.352	0.225
4	5.362	5.272	5.171	1.744	2.074	2.265	0.520	0.191
5	5.412	5.303	5.195	2.004	2.172	2.342	0.337	0.216
6	5.374	5.283	5.183	1.873	2.116	2.306	0.433	0.191

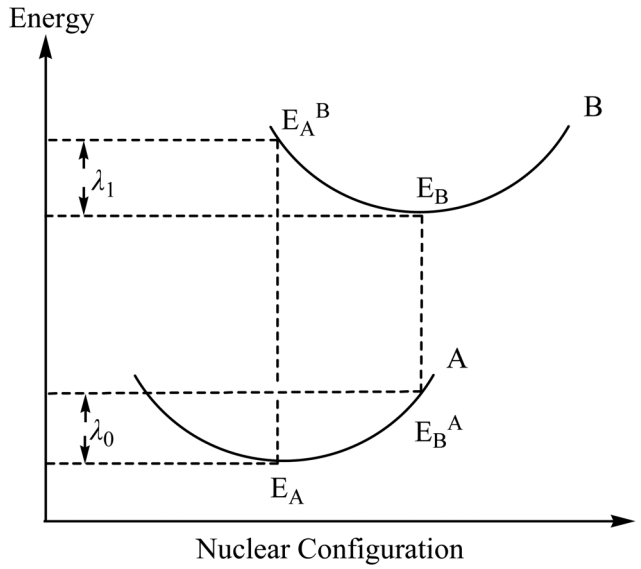

Fig. 3 Schematic description of the inner reorganization energy.

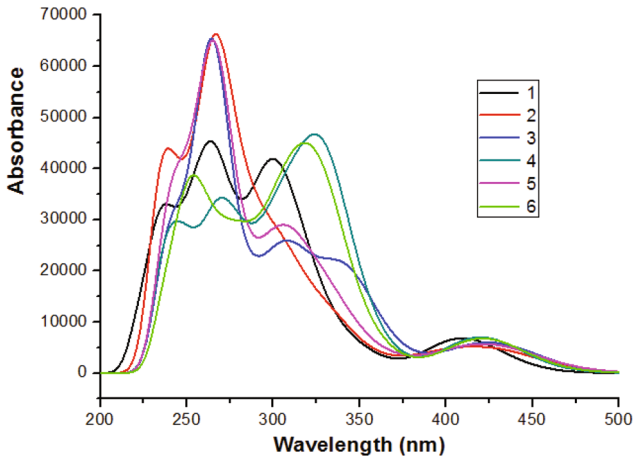

Fig. 4 Simulated absorption spectra in CH_2Cl_2 medium for complexes **1–6**.

energy difference between M (neutral molecule) and M^+ (cationic), using M^+ geometry. The electron extraction potential (EEP) has also been calculated, which is the energy difference between M and M^- (anionic), using M^- geometry. The inner reorganization energy for hole (λ_h) and electron transport (λ_e) can be evaluated as follows:

$$\lambda_h = IP_v - HEP \quad (3)$$

$$\lambda_e = EEP - EA_v \quad (4)$$

The reorganization energy (λ) can be approximately used to estimate the charge transport rate and balance between holes and electrons and is listed in Table 2. The reorganization energies for hole transport (λ_e) of complexes **1–6** are larger than those for electron transport (λ_h), which reveals that the hole transporting performances of these complexes are better than electron transporting performances. The difference between λ_h and λ_e for **2** is the smallest among complexes **1–6**, so hole and electron transfer balance could be easily achieved in the emitting layer, which is the key factor for efficient OLED materials.

3.4 Absorption spectra

On the basis of the optimized ground state geometries, the absorption spectra of complexes **1–6** have been calculated by using the PCM-TD-PBE0 method in CH_2Cl_2 medium. The vertical electronic excitation energies, oscillator strengths (f), dominant orbital excitations and their assignments of the singlet excited state are presented in Table S7 (ESI†). The simulated absorption spectral properties of complexes **1–6** are sketched in Fig. 4.

It can be seen from Table S7† that the lowest lying singlet → singlet absorption of **1–6** is located at 414 nm (f = 0.0621), 434 nm (f = 0.0473), 434 nm (f = 0.0552), 421 nm (f = 0.0824), 436 nm (f = 0.0475) and 425 nm (f = 0.0703), respectively. The calculated 434 nm absorption for complex **3** can be comparable to the available experimental value of 418 nm.[24] However, from the article by Feng *et al.*,[24] it can be seen that there is an obvious difference between the measured value and the calculated lowest lying singlet → singlet absorption wavelength of 486.7 nm for complex **3**. It is obvious that the lowest lying singlet → singlet absorption of complexes **2** and **3** is red-shifted compared to that of **1**, which is consistent with the variation rule of the $\Delta E_{L\rightarrow H}$ values. The lowest lying absorptions for complexes **1–6** mainly have the HOMO → LUMO transition configuration contributing to the $S_0 \rightarrow S_1$ state, and they have the same transitions; for example, the lowest energy absorption of **1** is characterized as metal-to-ligand charge transfer (MLCT)/ligand-to-ligand charge transfer (LLCT)/intra-ligand charge transfer (ILCT) [d(Ir) + π(L1 + L2) → π*(L1)] character. For complex **1**, the high-energy absorption is located at 295 nm, which is arising from S_{14} (HOMO−3 → LUMO and HOMO−1 → LUMO+2). From Table S1,† it can be seen that H−1 and H−3 are composed of 36% Ir(d) and 19% Ir(d), respectively. The absorption at 295 nm can be assigned to MLCT/LLCT/ILCT transition. The lowest lying absorptions of both **2** and **3** are at 434 nm, which is very close to that of **5**, that is, 436 nm. From Fig. 4 and Table S7,† it can be seen that complexes **2**, **3** and **5** possess not only similar absorption curves but close lowest-lying absorption wavelengths, oscillator strengths, and transition characters. For example, the lowest lying absorption of complex **2** can be characterized as a d(Ir) + π(L1 + L2) → π*(L1) transition with MLCT/LLCT/ILCT character. The lowest lying absorptions of **4** and **6** are 421 and 425 nm, respectively. Furthermore, as for **4** and **6**, they possess a similar absorption line shape, in which there are the maximum peaks at about 320 nm in the absorption spectra. From the abovementioned discussion, it can be drawn that changing the L1 and L2 ligands by different methods, such as, altering the position and number of the incorporated electron-withdrawing fluorine substituents, can adjust the absorption properties of complexes **1–6**.

.5 Phosphorescence in CH_2Cl_2 medium

In general, TDDFT systematically underestimates the transition energies, but it reproduces the general trend. To check the computational method, six different density functionals (B3LYP,[33] CAM-B3LYP,[34] M052X,[35] M062X,[36] BP86[37] and PBE0[38]) were used to calculate the emission of complex **3**. A better agreement with experimental data was obtained for M062X relative to the other five functionals. The calculated emission wavelengths for **3** at B3LYP, CAM-B3LYP, BP86, M052X, M062X and PBE0 levels are 720, 791, 715, 681, 633 and 749 nm, respectively, with the deviations of 88, 159, 83, 49, 1 and 117 nm from the measured value of 632 nm.[24] Obviously, the M062X functional yielded a more satisfactory result. So, we have employed the M062X functional for further emission spectral calculations. On the basis of the optimized triplet excited-state geometries, the emission properties of complexes **1–6** in CH_2Cl_2 solution obtained using the TDDFT method are shown in Table 3. The plots of the molecular orbitals related to emissions of complexes **1–6** are presented in Table 4. Besides, partial frontier molecular orbital compositions (%) of complexes **1–6** in the triplet excited states are presented in Table S8 (ESI†).

Table 3 shows that the calculated lowest energy emissions of complexes **1–6** are located at 617, 492, 633, 634, 491 and 491 nm, respectively. The calculated emission wavelength of 561.8 nm for complex **3** by Feng *et al.*[24] has a significant deviation from the measured value, which is not as good as our theoretical method. It can be seen that complex **2** has the smallest emission wavelength among complexes **1**, **2** and **3** with a similar molecular structure. It can be seen that the emission wavelengths of complexes **2**, **5** and **6** are in the range of 490 nm whereas those of complexes **1**, **3** and **4** are in the range of 600 nm. Indeed, it cannot be concluded that there is a clear correlation between the phosphorescent emissions and the substitution of ligands. Interestingly, comparing complex **4** with **5**, the only difference in the molecular structure is the different fluorine substitution position, in which there is an about 143 nm difference in the emission wavelength. It can be seen from Table 3 that complexes **1–6** have the same emission transition characters. For example, complex **1** has the triplet metal-to-ligand charge transfer (^{3}MLCT)/triplet ligand-to-

Table 3 Phosphorescent emissions of complexes **1–6** in CH_2Cl_2 using the TDDFT calculations, together with the experimental wavelength (nm) available

	λ (nm)/E (eV)	Configuration	Assignment	Nature	Expt.[a]
1	617/2.01	L → H (81%)	π*(L1 + L2) → d(Ir) + π(L1)	^{3}MLCT/^{3}LLCT/^{3}ILCT	
		L+1 → H (12%)	π*(L1 + L2) → d(Ir) + π(L1)	^{3}MLCT/^{3}LLCT/^{3}ILCT	
2	492/2.51	L → H (55%)	π*(L1) → d(Ir) + π(L1 + L2)	^{3}MLCT/^{3}LLCT/^{3}ILCT	
		L → H−2 (26%)	π*(L1) → π(L1 + L2)	^{3}LLCT/^{3}ILCT	
3	633/1.95	L → H (76%)	π*(L1 + L2) → d(Ir) + π(L2)	^{3}MLCT/^{3}LLCT/^{3}ILCT	632[a]
		L+1 → H (16%)	π*(L1 + L2) → d(Ir) + π(L2)	^{3}MLCT/^{3}LLCT/^{3}ILCT	
4	634/1.95	L → H (87%)	π*(L2) → d(Ir) + π(L1 + L2)	^{3}MLCT/^{3}LLCT/^{3}ILCT	
5	491/2.52	L → H (47%)	π*(L1) → d(Ir) + π(L1 + L2)	^{3}MLCT/^{3}LLCT/^{3}ILCT	
		L+1 → H (17%)	π*(L2) → d(Ir) + π(L1 + L2)	^{3}MLCT/^{3}LLCT/^{3}ILCT	
		L → H−2 (10%)	π*(L1) → π(L1 + L2)	^{3}LLCT/^{3}ILCT	
6	491/2.52	L → H (52%)	π*(L1) → d(Ir) + π(L1 + L2)	^{3}MLCT/^{3}LLCT/^{3}ILCT	
		L → H−2 (18%)	π*(L1) → π(L1 + L2)	^{3}LLCT/^{3}ILCT	

[a] Ref. 24.

Table 4 The frontier molecular orbital contours related to the lowest energy phosphorescence emissions of complexes **1–6**

	1	**2**	**3**	**4**	**5**	**6**
L+1	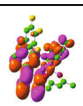		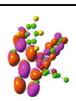		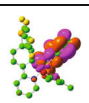	
L	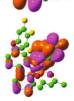	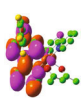	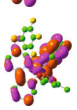			
H	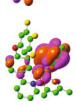		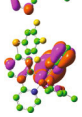	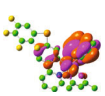	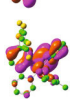	
H−2						

ligand charge transfer (^{3}LLCT)/triplet intraligand charge transfer (^{3}ILCT) transition characters. The theoretical results show that a slight change of the molecular structure could result in an obvious difference in the phosphorescence emission properties. As shown in Table 4 and Table S8,† the HOMOs of complexes **1–6** are localized on the Ir atom and L2 ligand. For example, the HOMO of complex **1** is distributed on the Ir (25%) and L2 ligand (65%). The LUMOs of complexes **1–6** have different distributions, except for the LUMOs of **2**, **5** and **6** which have the same distribution character, that is, L1 ligand (94%).

4. Conclusions

In this study, we have used the DFT and TDDFT methods to investigate the ground and excited state structures and absorption and emission spectra of six iridium(III) complexes with two ppy-type ligands and one acetylacetone anion around the Ir center. The aim is to investigate the effect of introducing different atoms and changing the position and number of the incorporated fluorine atoms on the electronic structure and photophysical properties. The lowest lying absorptions for all studied complexes possess the HOMO → LUMO transition configuration with MLCT/LLCT/ILCT [d(Ir) + π(L1 + L2) → π* (L1)] character. Complexes **2**, **3** and **5** have a similar absorption line shape. The calculated emission wavelength of 633 nm for **3** at the M062X level is in good agreement with the experimental value. We hope that this research work can provide some information to design good iridium complexes as phosphorescent emitters.

Conflicts of interest

The authors have no conflicts to declare.

Acknowledgements

The authors are grateful to the financial aid from the National Natural Science Foundation of China (Grant No. 31971252), the Program of Science and Technology Development Plan of Jilin Province (Grant No. 20170204044GX) and the Science and Technology Research Project for the Thirteenth Five-year Plan of Education Department of Jilin Province of China (Grant No. JJKH20181021KJ and JJKH20170604KJ).

References

1 K. Traskovskis, A. Ruduss, V. Kokars, I. Mihailovs, N. Lesina and A. Vembris, *New J. Chem.*, 2019, **43**, 37.
2 A. Schinabeck, N. Rau, M. Klein, J. Sundermeyer and H. Yersin, *Dalton Trans.*, 2018, **47**, 17067.
3 B. Jiang, X. W. Ning, S. L. Gong, N. Jiang, C. Zhong, Z. H. Lu and C. L. Yang, *J. Mater. Chem. C*, 2017, **5**, 10220.
4 X. H. Shang, D. M. Han, L. H. Zhao, L. J. Li and S. H. Lv, *Photochem. Photobiol. Sci.*, 2019, **18**, 1075.
5 H. Shin, J. H. Lee, C. K. Moon, J. S. Huh, B. Sim and J. J. Kim, *Adv. Mater.*, 2016, **28**, 4920.
6 C. Y. Lu, M. Jiao, W. K. Lee, C. Y. Chen, W. L. Tsai, C. Y. Lin and C. C. Wu, *Adv. Funct. Mater.*, 2016, **26**, 3250.
7 M. A. Baldo, D. F. O'Brien, Y. You, A. Shoustikov, S. Sibley, M. E. Thompson and S. R. Forrest, *Nature*, 1998, **395**, 151.
8 D. M. Han, P. Gong, S. H. Lv, L. H. Zhao and H. N. Zhao, *Mol. Phys.*, 2018, **116**, 1218.
9 Q. Zhao, S. J. Liu and W. Huang, *Macromol. Rapid Commun.*, 2010, **31**, 794.
10 Z. Q. Chen, Z. Q. Bian and C. H. Huang, *Adv. Mater.*, 2010, **22**, 1534.
11 H. F. Shi, Y. Nakai, S. J. Liu, Q. Zhao, Z. F. An, T. Tsuboi and W. Huang, *J. Phys. Chem. C*, 2011, **115**, 11749.
12 Y. F. Hu, A. Maclennan and T. K. Sham, *J. Lumin.*, 2015, **166**, 143.
13 I. Taidakov, S. Ambrozevich, R. Saifutyarov, K. Lyssenko, R. Avetisov, E. Mozhevitina, A. Khomyakov, M. Khrizanforov, Y. Budnikova and I. Avetissov, *J. Organomet. Chem.*, 2018, **867**, 253.
14 H. Brahim, B. Haddad, M. Boukabene, S. Brahim and B. Ariche, *Comput. Theor. Chem.*, 2017, **1101**, 8.
15 V. Cherpak, P. Stakhira, B. Minaev, G. Baryshnikov, E. Stromylo, I. Helzhynskyy, M. Chapran, D. Volyniuk, D. Tomkuté-Lukšienė, T. Malinauskas, V. Getautis, A. Tomkeviciene, J. Simokaitiene and J. V. Grazulevicius, *J. Phys. Chem. C*, 2014, **118**, 11271.
16 X. Li, B. Minaev, H. Ågren and H. Tian, *Eur. J. Inorg. Chem.*, 2011, **2011**, 2517.
17 D. Liu, L. J. Deng, W. Li, R. J. Yao, D. L. Li, M. Wang and S. F. Zhang, *Adv. Opt. Mater.*, 2016, **4**, 864.
18 F. L. Zhang, C. F. Si, X. B. Dong, D. H. Wei, X. Yang, K. P. Guo, B. Wei, Z. Y. Li, C. Zhang, S. Z. Li, B. Zhai and G. X. Cao, *J. Mater. Chem. C*, 2017, **5**, 9146.
19 G. P. Tan, L. Q. Wang, S. S. Wang, P. Liu, H. B. Fan, C. L. Ho, D. G. Ma and W. Y. Wong, *Dyes Pigm.*, 2019, **160**, 717.
20 J. Park, Y. H. Lee, J. Y. Ryu, J. Lee and M. H. Lee, *Dalton Trans.*, 2016, **45**, 5667.
21 S. Kumar, Y. Hisamatsu, Y. Tamaki, O. Ishitani and S. Aoki, *Inorg. Chem.*, 2016, **55**, 3829.
22 M. A. Esteruelas, E. Onate and A. U. Palacios, *Organometallics*, 2017, **36**, 1743.
23 L. Ding, C. X. Zang, H. T. Mao, G. G. Shan, L. L. Wen, H. Z. Sun, W. F. Xie and Z. M. Su, *Chem. Commun.*, 2018, **54**, 11761.
24 Z. Feng, D. Z. Wang, X. L. Yang, D. Y. Jin, D. K. Zhong, B. A. Liu, G. J. Zhou, M. F. Ma and Z. X. Wu, *Inorg. Chem.*, 2018, **57**, 11027.
25 P. Hohenberg and W. Kohn, *Phys. Rev.*, 1964, **136**, B864.
26 C. Adamo and V. Barone, *J. Chem. Phys.*, 1999, **110**, 6158.
27 P. J. Hay and W. R. Wadt, *J. Chem. Phys.*, 1985, **82**, 270.
28 P. J. Hay and W. R. Wadt, *J. Chem. Phys.*, 1985, **82**, 299.
29 M. J. Frisch, G. W. Trucks, H. B. Schlegel, G. E. Scuseria, M. A. Robb, J. R. Cheeseman, G. Scalmani, V. Barone,

B. Mennucci, G. A. Petersson, H. Nakatsuji, M. Caricato, X. Li, H. P. Hratchian, A. F. Izmaylov, J. Bloino, G. Zheng, J. L. Sonnenberg, M. Hada, M. Ehara, K. Toyota, R. Fukuda, J. Hasegawa, M. Ishida, T. Nakajima, Y. Honda, O. Kitao, H. Nakai, T. Vreven, J. A. Montgomery, J. E. Peralta, F. Ogliaro, M. Bearpark, J. J. Heyd, E. Brothers, K. N. Kudin, V. N. Staroverov, R. Kobayashi, J. Normand, K. Raghavachari, A. Rendell, J. C. Burant, S. S. Iyengar, J. Tomasi, M. Cossi, N. Rega, N. J. Millam, M. Klene, J. E. Knox, J. B. Cross, V. Bakken, C. Adamo, J. Jaramillo, R. Gomperts, R. E. Stratmann, O. Yazyev, A. J. Austin, R. Cammi, C. Pomelli, J. W. Ochterski, R. L. Martin, K. Morokuma, V. G. Zakrzewski, G. A. Voth, P. Salvador, J. J. Dannenberg, S. Dapprich, A. D. Daniels, O. Farkas, J. B. Foresman, J. V. Ortiz, J. Cioslowski and D. J. Fox, *Gaussian 09, Revision A.02*, Gaussian Inc., Wallingford, CT, 2009.

30 N. S. Hush, *J. Chem. Phys.*, 1958, **28**, 962.

31 M. Malagoli and J. L. Brédas, *Chem. Phys. Lett.*, 2000, **327**, 13.

32 B. C. Lin, C. P. Cheng, Z. Ping and M. Lao, *J. Phys. Chem. A*, 2003, **107**, 5241.

33 T. A. Niehaus, T. Hofbeck and H. Yersin, *RSC Adv.*, 2015, **5**, 63318.

34 C. Cramer and D. Truhlar, *Solvent Effects and Chemical Reactivity*, Kluwer, Dordrecht, The Netherlands, 1996.

35 Y. Zhao, N. E. Schultz and D. G. Truhlar, *J. Chem. Theory Comput.*, 2006, **2**, 364.

36 Y. Zhao and D. G. Truhlar, *Theor. Chem. Acc.*, 2008, **120**, 215.

37 J. P. Perdew, *Phys. Rev. B: Condens. Matter Mater. Phys.*, 1986, **33**, 8822.

38 J. P. Perdew, K. Burke and M. Ernzerhof, *Phys. Rev. Lett.*, 1996, **77**, 3865.

